6-27-2001

Complex Effects Arising in Smoke Plume Simulations due to Inclusion of Direct Emissions of Oxygenated Organic Species from Biomass Combustion

Sherri A. Mason
University of Montana - Missoula

Richard J. Field
University of Montana - Missoula

Robert J. Yokelson
University of Montana - Missoula, bob.yokelson@umontana.edu

Michael A. Kochivar
University of Montana - Missoula

Mark R. Tinsley
University of Montana - Missoula

JOURNAL OF GEOPHYSICAL RESEARCH, VOL. 106, NO. D12, PAGES 12,527–12,539, JUNE 27, 2001

Complex effects arising in smoke plume simulations due to inclusion of direct emissions of oxygenated organic species from biomass combustion

Sherri A. Mason, Richard J. Field, Robert J. Yokelson, Michael A. Kochivar, and Mark R. Tinsley
The University of Montana, Missoula, Montana

Darold E. Ward and Wei Min Hao
Rocky Mountain Research Station, Missoula, Montana

Abstract. Oxygenated volatile organic species (oxygenates), including HCOOH, H_2CO, CH_3OH, $HOCH_2CHO$ (hydroxyacetaldehyde), CH_3COOH, and C_6H_5OH, have recently been identified by Fourier transform infrared measurements as a significant component of the direct emissions from biomass combustion. These oxygenates have not generally been included in the hydrocarbon-based initial emission profiles used in previous photochemical simulations of biomass combustion smoke plumes. We explore the effects of oxygenates on this photochemistry by using an established initial emission hydrocarbon profile and comparing simulation results obtained both with and without addition of the above six oxygenates. Simulations are started at noon and carried out for 30 hours in an expanding Lagrangian plume. After an initial transient period during which $[NO_x]$ falls rapidly, conditions within the oxygenated smoke plume are found to be strongly NO_x-sensitive, and the simulated final species profile is thus strongly dependent upon the $\Delta[NO]/\Delta[CO]$ initial emission profile. Oxygenate addition results in very significant and complex effects on net O_3 production, as well as on the relative amounts of long-lived HO_x and NO_x reservoir species (H_2O_2, organic hydroperoxides, HNO_3, and peroxyacetyl nitrate (PAN)) that are mixed into the surrounding atmosphere. Oxygenates may either increase or decrease net O_3 production (depending upon the initial $\Delta[NO]/\Delta[CO]$). However, they always increase H_2O_2 and organic hydroperoxide production as a result of increased rates of radical + radical reactions. These effects spring largely from accelerated removal of NO_x from the smoke plume due to increased radical concentrations resulting both from photolysis of oxygenates (mainly CH_2O) and from their relatively high reactivity. Predicted concentrations of H_2O_2, $\Delta[O_3]/\Delta[CO]$, $\Delta[NH_3]/\Delta[CO]$, and $\Delta[HCOOH]/\Delta[CO]$ are compared with some available measured values.

1. Introduction

Biomass combustion has long been known to inject significant quantities of CO_2, CO, CH_4, NO_x, nonmethane hydrocarbons (NMHC), and particulates into the atmosphere [*Crutzen and Andreae*, 1990]. However, recent ground-based and airborne Fourier transform infrared (FTIR) spectroscopic measurements have identified oxygenated organic compounds (oxygenates) as being important additional components of biomass combustion smoke, at levels comparable to NMHCs [*Griffith et al.*, 1991; *Yokelson et al.*, 1996a, 1996b, 1997, 1999a; *Goode et al.*, 1999, *Goode et al.*, 2000]. Other studies have confirmed these FTIR results [*McKenzie et al.*, 1995; *Worden et al.*, 1997; *Holzinger et al.*, 1999]. The major oxygenated species (formaldehyde (CH_2O), methanol (CH_3OH), acetic acid (CH_3COOH), formic acid (HCOOH), hydroxyacetaldehyde ($HOCH_2CHO$), and phenol (C_6H_5OH)) have not generally been included as substantial initial components in previous smoke-modeling efforts [*Chatfield and Delany*, 1990; *Richardson et al.*, 1991; *Keller et al.*, 1991; *Jacob et al.*, 1992; *Crutzen and Carmichael*, 1993; *Jacob et al.*, 1996; *Thompson et al.*, 1996; *Chatfield et al.*, 1996; *Koppmann et al.*, 1997; *Mauzerall et al.*, 1998; *Lee et al.*, 1998], particularly at the levels observed in the FTIR measurements, largely because they are not easily measured by more common analytical methods. Thus we report here a series of simulations designed to probe the impact of directly emitted oxygenated organic compounds on the early photochemistry of biomass combustion smoke plumes.

The major effect reported here from the inclusion of directly emitted oxygenates into smoke plume simulations results from their impact on the evolution of $[NO_x]$. NO_x and volatile organic compounds (VOC) are the two primary precursors of O_3 formation, and previous photochemical modeling studies have revealed the nonlinear relationship between their respective concentrations. From these studies, including analysis of the underlying chemical equations, the troposphere has been found to have two fundamentally different processing states: one in which O_3 formation increases with increasing $[NO_x]$ and is largely independent of [VOC], known as NO_x sensitive (limited) or low NO_x, and another in which O_3 production decreases with increasing $[NO_x]$ but in-

Paper Number 2001JD900003.
0148-0227/01/2001JD900003$09.00

creases with increasing [VOC], termed VOC sensitive (limited), NO_x saturated, or high NO_x [*Kleinman*, 1994; *Sillman*, 1999, and references therein]. Tropospheric photochemical models are often run under differing constant emission fluxes of VOC and NO_x (occasionally keeping the VOC/NO_x emission ratio constant) in order to determine which processing state a particular simulated event represents. The VOC emissions are normally assumed to be composed predominately of hydrocarbons (HC), and most VOC/NO_x modeling studies have focused on the effects of simply varying HC emission rates. Hence the modeling work reported here also focuses on the impact of the direct emission of oxygenated VOCs on VOC/NO_x-sensitive photochemistry.

We begin with a brief introduction to tropospheric photochemistry along with a discussion of the VOC and NO_x sensitive atmospheric processing states. In section 3 we describe the photochemical model used for these studies. Section 4 details our results (within the context of the VOC/NO_x sensitive photochemistry described in section 2) on the effect of oxygenated organic compounds on the product distribution profile within a biomass combustion smoke plume, including both O_3 and longer-lived pollutant reservoir species such as hydroperoxides and peroxyacyl nitrates (PAN). Section 5 gives a brief comparison of some of our numerical results to field measurements.

2. Tropospheric Photochemistry

2.1. General Description

Tropospheric gas phase photochemistry may be described as the photochemically driven, NO_x-catalyzed oxidation of CO and VOCs with the coproduction of O_3. The term VOC is used here to refer collectively to both oxygenated organic compounds and HCs. The catalytic photochemical reaction cycle is initiated and perpetuated by radical species, which are introduced into the troposphere via mainly photolytic radical initiation steps. Radical species, as well as NO_x, are removed (however, in some cases only temporarily) from the photochemical cycle through termination reactions, e.g., (1) - (5).

$$OH + NO_2 \rightarrow HNO_3 \quad (1)$$

$$RC(O)O_2 + NO_2 \rightarrow PANs \quad (2)$$

$$RO_2 + NO \rightarrow RONO_2 \quad (3)$$

$$HO_2 + HO_2 \rightarrow H_2O_2 + O_2 \quad (4)$$

$$RO_2 + HO_2 \rightarrow ROOH + O_2 \quad (5)$$

The first three reactions consume NO_x, as well as radical species, and will be referred to here as "Rad + NO_x" termination reactions, while the last two are radical-recombination reactions and will be referred to as "Rad + Rad" termination reactions [*Kleinman*, 1994]. The dominant termination reactions are determined by the relative availability of NO_x and radical species [*Kleinman*, 1994].

Rad + NO_x and Rad + Rad reactions have been defined above as consuming or removing radicals and NO_x from the photochemical cycle. In fact, most of the products formed in reactions (1) - (5), and other similar reactions, are long-term pollutant reservoir species. That is, they allow long-range transport of photochemically and thermally active species away from local events and into regional, even global, atmospheres to possibly reintroduce radicals or NO_x into the troposphere at a later time. Hence NO_x removal is used here to refer to the local effect, but the possible larger-scale implications should not be overlooked.

2.2. VOC/NO_x Sensitivity

The formation of O_3 in the troposphere, which is a central element of the photochemical cycle, results from the photolysis of NO_2. However, the majority of NO_x emissions into the atmosphere are in the form of NO, and the photolysis of NO_2 regenerates NO as well. Thus in order to obtain net cyclic O_3 formation, NO must be converted to NO_2 by a molecule other than O_3 itself. It is a primary role of peroxy radical species to perform this conversion via reactions such as (6):

$$RO_2 + NO \rightarrow RO + NO_2. \quad (6)$$

Either reactant may be in excess in these reactions, causing the system to be sensitive to the other.

In the VOC sensitive (high-NO_x) tropospheric state the emission of NO_x exceeds the production of radical species. Radicals are thus rapidly removed from the system, via reactions (1)-(3), limiting their availability to perform the NO-to-NO_2 conversion (as in reaction (6)) and inhibiting O_3 production. Overall the VOC sensitive state is characterized by a decrease in [O_3] with increasing [NO_x], while an increase in [VOC] increases radical production and therefore increases [O_3] [*Kleinman*, 1994; *Sillman*, 1999].

The NO_x sensitive (low NO_x) tropospheric processing state occurs under stoichiometric conditions in reactions such as (6) opposite to those of the VOC sensitive state. Rather than the NO-to-NO_2 conversion reactions being limited by radical availability, in the NO_x sensitive state O_3 production is limited by the availability of NO_x itself. Under such conditions, O_3 formation increases with increasing [NO_x] because radical species are readily available to convert NO to NO_2 [*Kleinman*, 1994]. Previous studies also have concluded that O_3 production in this state is largely independent of [VOC], presumably owing to a saturation effect in which an increase in radical species, which are already more available than NO_x, does not lead to an increase in NO-to-NO_2 reaction rate; hence little effect is observed on O_3 production [*Sillman*, 1999]. However, the simulations presented here illustrate that net O_3 formation can sometimes be VOC-dependent under NO_x-sensitive conditions owing to VOC-induced removal of NO_x leading to reductions in both O_3 destruction and production.

As a final note, it has frequently been observed in previous VOC/NO_x models that urban plumes undergo a transition from VOC sensitive (close to the city center) to NO_x-sensitive (in outlying, rural areas) photochemistry owing to removal of NO_x from the plume by photochemical processing, as well as by dilution [*Sillman*, 1999]. A similar phenomenon is noted here for biomass combustion smoke plumes.

2.3. Photochemistry of Oxygenates

The addition of oxygenated organic species into a tropospheric model where they had been previously ignored has considerable impact upon the predicted dominant reaction pathways and, hence, the resulting product distribution. This is due to the dependence of these pathways on the relative concentrations of NO_x and radical species. Unlike pure HCs, the degradation of some oxygenated organics, such as CH_2O and $HOCH_2CHO$, is initiated not only by OH attack, but also via direct photolysis. Thus the inclusion of these oxygenated compounds provides an additional direct source of radical species. Furthermore, oxygenated organic species are in general more reactive than are NMHC [*Finlayson-Pitts and Pitts*, 2000], causing an additional increase in radical species production through the general photochemical cycle itself. This increase in radical species production has complex effects on the production of O_3 and other photochemical products in a smoke plume where

the amount of NO_x varies but is limited to the relatively small concentrations (as compared to urban/industrial processes) initially introduced by the fire. While oxygenated compounds can increase the concentrations of radical species and the general level of photochemistry within a smoke plume, therefore acting to increase O_3 production, they also can speed the titration of NO_x out of the smoke plume via Rad + NO_x termination reactions, slowing O_3 production and altering the product distribution profile. Thus the net effect of directly emitted oxygenated organic compounds on O_3 and other photochemical products results from a complex balancing of these two effects and may either be positive or negative.

3. Photochemical Model

All simulations reported here were performed by using the National Center for Atmospheric Research (NCAR) Master Mechanism (MM) [*Madronich and Calvert*, 1989]. The MM is a zero-dimensional tropospheric box model which explicitly describes (in ~5000 chemical reactions) the photochemistry of alkanes and aromatics up to C_8, alkenes up to C_4, and two biogenic species, isoprene and α-pinene. A subset of these reactions may be selected by specifying an initial profile of chemical species. The model used here has been simplified by excluding HCs greater than C_4 and therefore contains only 702 reactions (79 photolytic) involving 267 species. Included in the MM package is an algorithm that calculates the actinic flux as a function of wavelength and time of day for given atmospheric conditions, altitude, location, and time of year [*Madronich*, 1987]. This actinic flux is then used to calculate appropriate photolytic rate constants as a function of time of day based upon the spectra (cross sections and quantum yields) of absorbing species. In order to represent smoke processing during the tropical dry season (where 80% of biomass burning is reported to occur [*Hao and Liu*, 1994]), photolysis rates are calculated here for 13°S and 27°E (i.e., southern Africa) at 1-km altitude on August 31. Atmospheric conditions are based on the U.S. Standard Atmosphere (1976) using clear-sky conditions, a total O_3 column of 300 Dobson units, a surface albedo of 0.15, and a total aerosol optical depth of 0.21 at 340 nm.

Minor modifications were made to the MM in order to more accurately model the evolution of a biomass combustion smoke plume. The numerical integrator was upgraded to the Livermore solver for ordinary differential equations with sparse Jacobian techniques (LSODES) as originally described by *Hindmarsh* [1983]. LSODES is considered to be one of the most robust routines available to obtain solutions to stiff systems and has been used to evaluate the precision of a number of other methods [*Olcese and Toselli*, 1998]. Also, the formation of NH_4NO_3(s) aerosol from NH_3(g) and HNO_3(g) was incorporated owing to the significant direct production of NH_3(g) in biomass combustion. The rate of removal of NH_3(g) and HNO_3(g) is assumed to be diffusion controlled, e.g., a reaction coefficient k equal to 10.5 $ppm^{-1}\,min^{-1}$ when $[NH_3(g)][HNO_3(g)] > [NH_3(g)]_{eq}[HNO_3(g)]_{eq}$, and zero otherwise. The thermodynamic equilibrium constant, K_{eq} (= $[NH_3(g)]_{eq}[HNO_3(g)]_{eq}$), for NH_4NO_3(s) is 3.07×10^{-6} ppm^2 at 297 K [*Seinfeld and Pandis*, 1998].

As opposed to most previous VOC/NO_x models, which used an Eulerian box model approach [*Sillman*, 1999, and references therein], the simulations reported here use a Lagrangian model. In the Eulerian scheme a spatial grid (each subsection with its own constant emissions of O_3 precursors) is fixed, and the flux and chemical behavior of an air mass moving through the grid is evaluated. Conversely, the Lagrangian approach models the evolution of a moving parcel of air from an initial set of emitted species concentrations [*Brasseur et al.*, 1999]. This method is particularly useful in the case of a heavily polluted plume moving away from a near point source where the initial profile of species react, essentially in a closed system, as the plume evolves. Thus a Lagrangian model does not utilize constant emission rates. This is an especially important distinction to make in regard to NO_x because it is continually supplied in Eulerian models (albeit to "fresh" air masses), while in the simulations reported here NO_x concentrations are limited to the initial concentrations within the smoke plume, with relatively minor contributions early in the plume evolution from the ambient air.

3.1. Continuous Plume Dilution

The atmospheric dilution of plumes has a substantial impact on predicted species concentrations [*Kley*, 1997; *Mauzerall et al.*, 1998; *Poppe et al.*, 1998]. Species concentrations within the smoke plume are modeled here within a well-mixed box which expands as it evolves. Concentrations within the box, therefore, change by photochemical reactions, as described by the MM, and by dilution with ambient air. The box has fixed height h (=1 km), fixed length l (=1 km), but variable width $y(t)$. The initial plume width $y(0)$ increases to $y(t)$ in time t, affecting species concentrations C_i by dilution with adjacent ambient air concentrations C_i^a. Following *Seinfeld and Pandis* [1998], at time t, when the box has width $y(t)$, a further increase in y of Δy yields the mass balance equation (7):

$$(C_i + \Delta C_i)[y(t) + \Delta y] = C_i\, y(t) + C_i^a\, \Delta y. \tag{7}$$

Neglecting the second-order term, $\Delta C_i\, \Delta y$, dividing by Δt, and taking the limit $\Delta t \to 0$ yield equation (8) for the instantaneous effect of plume widening on C_i:

$$\frac{dC_i}{dt} = -\frac{1}{y(t)}\frac{d[y(t)]}{dt}(C_i - C_i^a). \tag{8}$$

Equation (8) is of the same form as that used by *Poppe et al.* [1998]. The form of $y(t)$ is assumed to be $y(t) = [y(0)^2 + 8K_y t]^{1/2}$ obtained with reference to the Gaussian solution to the Fickian diffusion equation, $d\sigma/dt = K_y/\sigma$ [*Csanady*, 1973], by setting the plume width $y(t)$, equal to twice the Gaussian variance σ [*Sillman et al.*, 1990]. Substitution of $y(t)$ into (8) leads to (9):

$$\frac{dC_i}{dt} = -\frac{4K_y}{[y(0)^2 + 8K_y t]}(C_i - C_i^a). \tag{9}$$

Equation (9) is incorporated into the MM such that all species concentrations are diluted by their corresponding ambient concentrations at every time step. The right-hand side of (9) goes to zero as $t \to \infty$ and $(C_i - C_i^a) \to 0$. The parameter K_y is the cross-flow (horizontal) diffusion coefficient, which was determined here by fitting the dilution rates of the excess (over ambient) CO and CO_2 mixing ratios (ΔCO and ΔCO_2) to those estimated from observations on large isolated plumes by *Babbitt et al.* [1998] and *Goode et al.* [2000]. Based upon this curve fitting and using an initial plume width $y(0)$ of 1-km, K_y is set to 3.33×10^{-3} km^2/min, consistent with values of *Gifford* [1982] for plumes of comparable initial width.

3.2. Ambient and Initial Smoke Species Concentrations

3.2.1. Ambient. Diurnal variations in ambient concentrations of all species, C_i^a, were estimated by running the MM with a constant profile of trace gas concentrations (Table 1) typical of a

Table 1. Ambient Concentrations Used in Smoke-Plume Dilution

Name	Formula	Total Concentration (ppbv)
Nitrogen	N_2	7.8×10^8
Nitrogen Dioxide	NO_2	1
Nitric Oxide	NO	0.05
Nitrous Oxide	N_2O	320
Dinitrogen Pentoxide	N_2O_5	0.005
Nitric Acid	HNO_3	0.2
Nitrous Acid	HNO_2	0.03
Ammonia	NH_3	0.1
Peroxyacetyl Nitrate	PAN	0.05
Hydrogen Cyanide	HCN	0.19
Methane	CH_4	1650
Ethane	C_2H_6	13.50
Ethene	C_2H_4	11.10
Ethyne (Acetylene)	C_2H_2	8.65
Propane	C_3H_8	18.70
Propene	C_3H_6	2.6
Methanol	CH_3OH	0.5
Acetic Acid	CH_3COOH	2.1
Formic Acid	HCOOH	5.4
Formaldehyde	CH_2O	9.1
Carbon Dioxide	CO_2	3.5×10^5
Carbon Monoxide	CO	200
Carbonyl Sulfide	OCS	0.5
Sulfur Dioxide	SO_2	0.2
Oxygen	O_2	2.1×10^8
Ozone	O_3	29.30
Hydrogen Peroxide	H_2O_2	0.690
Water	H_2O	1.0×10^7
Hydrogen	H_2	500

rural environment [*Finlayson-Pitts and Pitts*, 1986; *Seinfeld and Pandis*, 1998] until a stable diurnal cycle in all intermediate species was achieved. Ambient profiles for a 24-hour day were then tabulated at 3-min resolution, and linear interpolation methods were used at intermediate times. It is important to note that as time increases, the ambient concentrations become a more important component of the calculated smoke plume concentrations.

3.2.2. Initial smoke species concentrations. Initial concentrations within the smoke plume are chosen to approximate conditions just above a large biomass fire with a ΔCO_2 of 100 ppmv and $\Delta CO/\Delta CO_2 = 7$ %. Other initial concentrations were scaled to either ΔCO_2 or ΔCO depending upon whether a particular species results mainly from flaming or smoldering combustion [*Yokelson et al.*, 1996a]. An initial species profile (Table 2) for fresh smoke based upon *Lobert et al.* [1991], not including oxygenates and referred to here as "No Oxy," is used as a standard. Simulations were then conducted with all of the six oxygenates (CH_2O, CH_3OH, $HOCH_2CHO$, CH_3COOH, HCOOH, and C_6H_5OH) added at the levels observed on average by *Yokelson et al.* [1996a] (except for phenol, whose concentration represents a high-end limit) in a profile referred to as "All Oxy" (Table 2), and with perturbed values of initial hydrocarbons used in order to evaluate the VOC/NO_x sensitivity. The No-Oxy profile is similar to that used in most previous smoke plume models, while the All-Oxy profile includes the influence of oxygenated organic compounds. In order to represent a range of typical values for real biomass combustion [*Yokelson et al.*, 1996a], all simulations were carried out at values of $\Delta[NO]_0/\Delta[CO]_0$ of both 1 and 2% (Table 2). The 1% $\Delta[NO]_0/\Delta[CO]_0$ emission ratio is representative of smoldering combustion, while 2% $\Delta[NO]_0/\Delta[CO]_0$ is more descriptive of an average combustion situation (flaming combustion yields an upper limit $\Delta[NO]_0/\Delta[CO]_0$ of 4-6%) [*Yokelson et al.*, 1999b]. This design allows not only for analysis of the effect of changing initial [VOC] via an increase of initial hydrocarbons, as well as by the addition of initial concentrations of oxygenated organic species to the smoke profile, but also for the effect of changing initial [NO_x].

4. Results and Discussion

Smoke plume simulations were started at 1200 (noon) and ran for 30 hours. The most dramatic changes occur within the first few hours when the sun is high and the plume is relatively concentrated. Typical simulated time profiles for [O_3] are shown in Figure 1, and the absolute concentrations of several species at 1400 on days 1 and 2 are listed in Table 3 for each of the four emission scenarios. Insight into the effects of oxygenated organic compounds upon early smoke plume photochemistry are obtained by comparing results from All-Oxy simulations to those from No-Oxy simulations. We report here the relative changes in overall average reaction rates, overall average concentrations, and total species production at both the first-day maximum and final 42-hour values (obtained by multiplying the specified concentrations by the plume volume at that time). Exact numerical values are undoubtedly model-dependent [*Olson et al.*, 1997], but we believe these relative values give a reliable account of the effect of the oxygenated organic species on smoke plume photochemistry.

Table 2. Actual Initial Concentrations in the Smoke Plume (i.e., at 1200 Noon of First Day) for the No-Oxy and All-Oxy Cases

Name	Formula	Total Concentration (ppbv)
Nitrogen	N_2	7.8×10^8
Nitrogen Dioxide	NO_2	37.60
Nitric Oxide	NO	75.25 (1%) or 150.5 (2%)
Nitrous Oxide	N_2O	335.04
Dinitrogen Pentoxide	N_2O_5	0.005
Nitric Acid	HNO_3	0.2
Nitrous Acid	HNO_2	0.03
Ammonia	NH_3	150.50
Peroxyacetyl Nitrate	PAN	0.05
Hydrogen Cyanide	HCN	15.20
Methane	CH_4	2260
Ethane	C_2H_6	61.10
Ethene	C_2H_4	161.6
Ethyne (Acetylene)	C_2H_2	56.20
Propane	C_3H_8	28.80
Propene	C_3H_6	35.80
Methanol	CH_3OH	0.50 (No Oxy) or 150.9 (All Oxy)
Phenol	C_6H_5OH	0 (No Oxy) or 56.10 (All Oxy)
Acetic Acid	CH_3COOH	2.10 (No Oxy) or 152 (All Oxy)
Formic Acid	HCOOH	5.40 (No Oxy) or 61.5 (All Oxy)
Formaldehyde	CH_2O	9.10 (No Oxy) or 159.5 (All Oxy)
Hydroxyacetaldehyde	$CH_2(OH)CHO$	1.50 (No Oxy) or 57.6 (All Oxy)
Carbon Dioxide	CO_2	4.5×10^5
Carbon Monoxide	CO	7200
Carbonyl Sulfide	OCS	49.30
Sulfur Dioxide	SO_2	49.00
Oxygen	O_2	2.1×10^8
Ozone	O_3	29.30
Hydrogen Peroxide	H_2O_2	0.690
Water	H_2O	1.0×10^7
Hydrogen	H_2	650.4

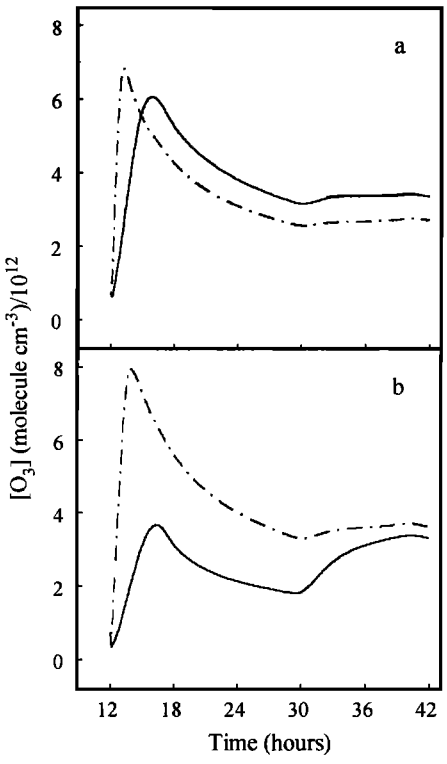

Figure 1. Simulated O_3 concentration (molecules/cm^3/10^{12}) versus time (hours). No Oxy, solid lines; All Oxy, dotted-dashed lines. (a) $\Delta[NO]_0/\Delta[CO]_0$ = 1%; (b) $\Delta[NO]_0/\Delta[CO]_0$ = 2%. Simulations were started at 1200 (noon) and ran for 30 hours with sunset occurring at ~1800 hours on the first day and sunrise occurring at ~0600 on the second day. The decline in concentration after ~16 hours is mainly associated with dilution of the smoke plume.

4.1. VOC/NO_x Sensitivity

The addition of direct emission of oxygenated organic species has a significant impact upon the dominant mode of photochemical processing that occurs within a smoke plume. Table 4 details changes in the No-Oxy and All-Oxy simulations of O_3 and OH production at the first-day maximum owing to a perturbation of the initial concentrations of either hydrocarbons or NO_x. The decrease in production of both indicator species resulting from an increase in [NO_x], together with comparable [OH] or increased [O_3] values resulting from an increase in hydrocarbon concentration, characterize the No-Oxy simulations as VOC sensitive. In contrast, the photochemistry within the All-Oxy simulations is found to be NO_x sensitive, as is demonstrated by a substantial increase in production of O_3 and OH with increasing initial [NO_x]. Thus inclusion of oxygenated organics causes the dominant photochemistry within the smoke plume to change from VOC to NO_x sensitive.

The dominance of VOC sensitive processing can be visualized by looking at the fraction of radicals lost via reaction with NO_x, as opposed to reaction with other radicals (Rad + NO_x and Rad + Rad being the two primary pathways for radical loss in the troposphere). *Kleinman et al.* [1994, 1997]and *Daum et al.* [2000] have shown that the fraction of radicals lost via these two pathways provides a good indication of the sensitivity of O_3 production to O_3 precursors. Their analyses indicate that when the fraction of radicals lost via reaction with NO_x (L_N/Q) takes on a high value, and the fraction lost via Rad + Rad reactions (L_R/Q) is low ($\leq$ 0.15), then VOC sensitive photochemical processing is dominant. Likewise, when the L_N/Q fraction is low, and the L_R/Q fraction is high, then conditions are NO_x sensitive. Figure 2 shows both fractions for the simulations reported here. As expected, all simulations show the dominance of Rad + NO_x reactions at night due to nighttime NO_3 chemistry and reduced radical concentrations. However, by the second day all simulations show a diurnal variation of the classic VOC to NO_x sensitive transition that is expected as a plume evolves. An important difference among the traces, however, is the VOC to NO_x sensitive transition that occurs on the first day for the All-Oxy simulations, but which is not present in the No-Oxy simulations. Thus, while the No-Oxy simulations are dominated by VOC sensitivity, the All-Oxy simulations are primarily NO_x sensitive.

This alteration of dominate photochemical pathway has interesting consequences for the behavior of O_3 and OH, as well as for other photochemically important species. While increasing the initial concentration of hydrocarbons in the No-Oxy simulations leads to increased [O_3] with little change in [OH], typical of VOC sensitive chemistry [*Sillman*, 1999], a comparable increase in the initial concentrations of oxygenates (comparing the All-Oxy simulation to the No-Oxy simulation) leads to substantially decreased concentrations of both of these indicator species (Table 4). This effect seems to result from differences in the two photochemical processing regimes, and indicates that the more reactive and photochemically active oxygenated organics have a greater impact upon VOC/NO_x sensitivity than does simple hydrocarbons.

4.2. VOC-to-NO_x Sensitive Transition

As indicated earlier, evidence of a transition from VOC to NO_x sensitive chemistry, as has been reported for urban plumes, is apparent in the simulations reported here. *Sillman* [1995] recommends use of the [H_2O_2]/[HNO_3] ratio as a measurable (and therefore verifiable) indicator of VOC/NO_x sensitive chemistry in real atmospheres. This is because high concentrations of HNO_3 reflect VOC sensitive conditions in which Rad + NO_x termination reactions dominate [*Sillman*, 1995], while H_2O_2 results from Rad + Rad reactions, which are suppressed under VOC sensitive conditions but increase linearly with radical production in the NO_x sensitive state [*Kleinman*, 1994]. In All-Oxy simulations and the lower NO_x No-Oxy simulation the formation rate of HNO_3 reaches a maximum and dominates Rad + Rad reaction rates (which lead to hydroperoxide production) during the first hours of the simulations (Figure 3). The transition takes longer in the No-Oxy simulations (and does not occur at all in the higher NO_x No-Oxy case) than in the All Oxy simulations. After the first few hours, however, the Rad + Rad reaction rates exceed the HNO_3 production rate (Figure 3), indicating a shift from VOC sensitive to NO_x sensitive photochemical processing. The concentration profiles for total hydroperoxides also indicate that as the smoke plume ages beyond the first few hours, chemical processing tends to shift from VOC (decreasing hydroperoxide concentration) to NO_x sensitive (increasing hydroperoxide concentration) chemistry (Figure 4). Again this transition takes longer to occur in the No-Oxy simulations than in the All-Oxy simulations. While neither of these conditions defines the VOC sensitive state, they both serve as indicators that all smoke plume simulations reported here are controlled by VOC sensitive chemistry early in the simulation period.

4.3. Decrease in NO_x Lifetime

The passage from VOC to NO_x sensitive chemistry occurs owing to the removal of NO_x from the plume [*Sillman*, 1999]. The lifetime of NO_x, defined as the time over which [NO_x] falls to 1/*e*

Table 3. Actual Simulated Species Concentrations (ppbv) in an Aged Smoke Plume at 1400 on Day 1 and at 1400 on Day 2

Species	Total Concentrations at 1400 on Day 1 $\Delta[NO]_0/\Delta[CO]_0$ = 1%; $\Delta[NO]_0/\Delta[CO]_0$ = 2%				Total Concentrations at 1400 on Day 2 $\Delta[NO]_0/\Delta[CO]_0$ = 1%; $\Delta[NO]_0/\Delta[CO]_0$ = 2%			
	No Oxy	All Oxy	No Oxy	All Oxy	No Oxy	All Oxy	No Oxy	All Oxy
NO_2	26.6	1.25	57.3	6.24	0.52	0.37	0.68	0.61
NO	3.38	0.08	16.2	0.34	0.06	0.05	0.09	0.07
N_2O	328	328	327	328	322	322	322	322
N_2O_5	0.03	0.00	0.02	0.01	0.00	0.00	0.00	0.00
HNO_4	0.40	0.11	0.10	0.56	0.02	0.01	0.02	0.02
HNO_3	0.38	0.08	0.38	0.33	0.38	0.23	2.95	0.63
NH_3	54.5	53.7	56.9	32.8	8.36	13.8	1.04	5.11
NH_4NO_3 (Aerosol)	24.7	32.3	21.2	60.6	43.8	37.4	58.7	70.2
PAN	4.49	6.08	1.58	8.78	2.30	1.65	2.63	2.55
Hydroxy-PAN	1.24	6.89	0.50	8.63	0.68	0.71	0.84	1.08
All PAN Species	6.85	22.1	2.58	28.7	3.61	3.03	4.20	4.77
Mono-substituted Nitrophenol	0.00	3.89	0.00	3.13	0 00	0.07	0.00	0.00
Di-substituted Nitrophenol	0.00	1.45	0.00	3.03	0.00	2.19	0.00	2.14
HCN	7.53	7.52	7.53	7.52	2.48	2.48	2.48	2.48
CH_4	1947	1947	1948	1947	1742	1742	1742	1742
C_2H_6	36.3	36.3	36.5	36.1	19.8	20.1	19.9	19.8
C_2H_4	55.2	48.8	66.5	41.5	4.18	6.82	5.23	3.93
C_2H_2	30.8	30.6	31.3	30.1	13.8	14.4	13.9	13.8
C_3H_8	22.5	22.3	23.0	21.8	16.7	17.7	16.7	16.7
C_3H_6	3.94	2.49	7.80	1.45	0.08	0.12	0.07	0.08
CH_3OH	0.48	70.1	0.49	68.8	0.57	20.3	0.51	19.0
C_6H_5OH	0.00	3.09	0.00	1.12	0.00	0.00	0.00	0.00
CH_3COOH	2.17	73.1	2.15	72.1	2.23	23.1	2.13	22.1
HCOOH	6.50	34.4	6.34	34.2	7.78	16.5	7.53	16.0
CH_2O	39.6	55.1	30.2	59.5	5.01	6.17	5.97	5.89
$HOCH_2CHO$	5.51	14.8	4.50	12.5	1.29	2.35	1.43	1.50
CO	3609	3688	3614	3691	1281	1335	1286	1329
OCS	24.3	24.3	24.3	24.3	7.97	7.97	7.97	7.97
SO_2	21.7	20.8	22.7	20.1	4.67	5.26	4.98	4.53
O_3	172	251	85.1	322	138	110	133	148
H_2O_2	0.71	15.5	0.63	6.87	14.3	22.7	13.6	21.5
Organic Peroxides	4.38	9.23	5.08	5.26	7.28	10.7	6.32	8.33

of its initial value, is decreased by a factor of ~2 owing to the addition of oxygenates (Table 5). This dramatic decrease in the NO_x lifetime is perhaps the most important effect of the oxygenates for smoke plume photochemistry because it limits the time that NO_x is available to catalyze the production of O_3, thereby affecting the overall oxidizing ability within the smoke plume. As a side note, in the simulations reported here, $[NO_x]$ decreases because of dilution with ambient air, as well as by chemical reaction. Undoubtedly these results would differ if such a plume were to mix with NO_x-rich urban air rather than the relatively NO_x-poor ambient air used here.

Table 4. Effect of a Given Increase on Total Production (Plume Volume × Concentration) at the First Day Maximum

	Species	No Oxy	All Oxy
Increase NO_x	O_3	-36%	38%
	OH	-52%	30%
Increase Hydrocarbons	O_3	12%	7%
	OH	0.3%	-11%
Increase Oxygenated Organics	O_3	-28%	N/A[a]
	OH	-13%	N/A[a]

[a] N/A, not applicable.

4.4. Removal of NO_x

The early dominance of the Rad + NO_x termination reactions (Figure 2) leads to rapid removal of NO_x from the smoke plume. Figure 5 details the component reaction rates which make up the Rad + NO_x reactions. HNO_3 formation is typically the dominant fate of NO_x in the troposphere [*Seinfeld and Pandis*, 1998], and for the smoke plume simulations reported here the formation of HNO_3 (reaction (1)) indeed is the dominant Rad + NO_x reaction early in the plume lifetime (Figure 5). However, the production of PANs (reaction 2) and organic nitrates ($RONO_2$) (reaction 3) becomes the dominant NO_x sink as the plume evolves (Table 6). The addition of oxygenates leads to a decrease in the formation rates of organic nitrates, while the preference for PAN formation over HNO_3 production becomes more pronounced upon the addition of oxygenates (Figure 5, Table 6). This latter effect has also been noted by *Tanner et al.* [1988] and by *Singh et al.* [1995]. It results, we believe, from an increase in $RC(O)O_2$ radicals due to the oxidation of aldehyde (and ketone) components of the oxygenates, as well as from a decrease in available OH (which reacts with NO_2 to form HNO_3) due to increased VOC loading (Table 7). The removal of NO_x into either PANs or HNO_3 is a local effect which

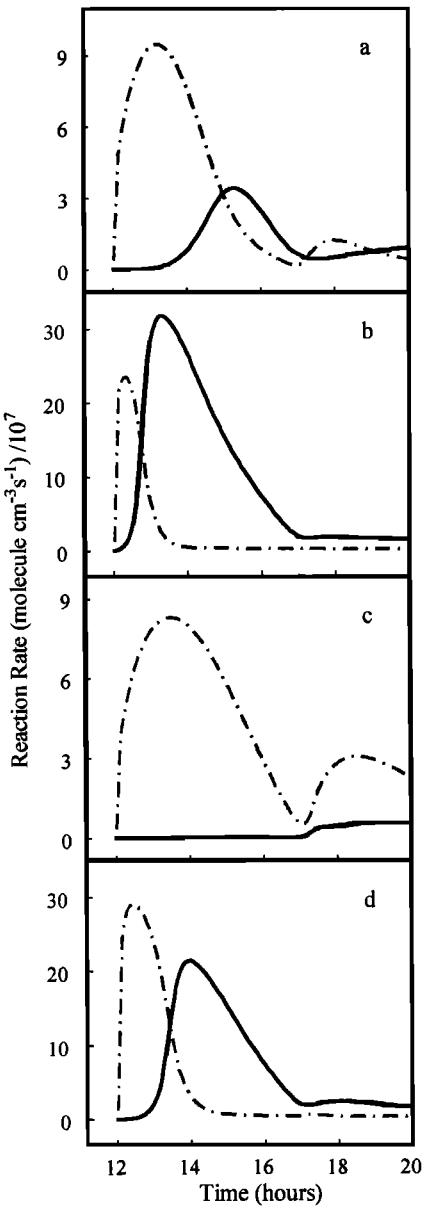

Figure 2. Simulated results for fraction of total radical removal via Rad + Rad reactions (solid lines) and Rad + NO_x reactions (dotted-dashed lines). Contributions from other radical removal pathways are not significant. (a) No Oxy with $\Delta[NO]_0/\Delta[CO]_0$ = 1%. (b) All Oxy with $\Delta[NO]_0/\Delta[CO]_0$ = 1%. (c) No Oxy with $\Delta[NO]_0/\Delta[CO]_0$ = 2%. (d) All Oxy with $\Delta[NO]_0/\Delta[CO]_0$ = 2%. Values of the Rad + Rad fraction greater than ~0.15 are indicative of NO_x sensitive conditions [*Kleinman*, 1994].

has regional and possibly even global implications owing to their role as NO_x reservoirs.

There is a significant added contribution to NO_x removal via Rad + NO_x reactions in All-Oxy simulations due to the formation of nitrophenols (reactions 10 and 11):

$$\cdot C_6H_4OH + NO_2 \rightarrow C_6H_4(OH)(NO_2) \quad (10)$$

$$\cdot C_6H_3(OH)(NO_2) + NO_2 \rightarrow C_6H_3(OH)(NO_2)(NO_2). \quad (11)$$

Unlike PANs and HNO_3, the possibility of rereleasing NO_x from nitrophenols is uncertain [*Seinfeld and Pandis*, 1998], and they are simply a sink for NO_x in the present model. Nevertheless, their added contribution helps offset decreases in the formation rates of HNO_3 (for the $\Delta[NO]_0/\Delta[CO]_0$ = 1% case only) and $RONO_2$ due to the addition of oxygenates (Table 6), and it is quite apparent that nitrophenols represent a significant addition to the product distribution profile within a biomass combustion smoke plume. These results suggest that the chemistry of these species should be studied further.

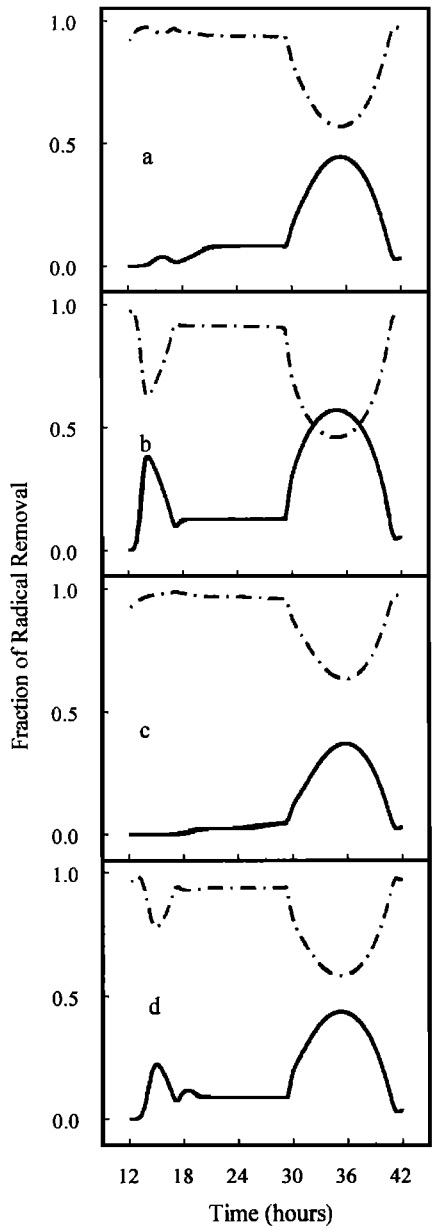

Figure 3. Calculated reaction rates (molecules/cm^3 s/10^7) versus time (hours) for Rad + Rad reactions (solid lines) and OH + NO_2 → HNO_3 (dotted-dashed lines). (a) No Oxy with $\Delta[NO]_0/\Delta[CO]_0$ = 1%. (b) All Oxy with $\Delta[NO]_0/\Delta[CO]_0$ = 1%. (c) No Oxy with $\Delta[NO]_0/\Delta[CO]_0$ = 2%. (d) No Oxy with $\Delta[NO]_0/\Delta[CO]_0$ = 2%. Most traces show HNO_3 formation to initially dominate, indicative of VOC sensitive conditions, but the radical recombination reactions eventually surpass HNO_3 formation, signifying a transition to NO_x sensitive conditions.

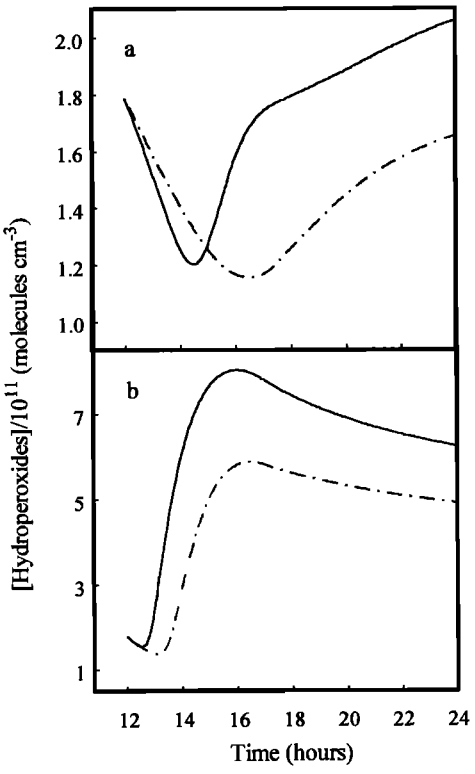

Figure 4. Simulated results for total hydroperoxide concentration (molecules/cm^3/10^{11}) versus time (hours) for $\Delta[NO]_0/\Delta[CO]_0 = 1\%$, (solid line) and $\Delta[NO]_0/\Delta[CO]_0 = 2\%$ (dotted-dashed line). (a) No Oxy. (b) All Oxy. Traces show an initial decline in total hydroperoxide concentration, consistent with VOC sensitive conditions, followed by a resurgence in their concentration corresponding to NO_x sensitive conditions. The [hydroperoxides] continue to increase on the second day (not shown).

4.5. Increase in Radical Species

The addition of oxygenates causes an overall increase in the removal of NO_x (via the Rad + NO_x termination reactions) owing to an increase in the concentrations of radical species, most notably HO_2 (Table 7). A portion of this increase in [HO_2] results from an increase in the photolysis of CH_2O (Table 6), which arises both from an increase in the initial concentration of it and its precursors (e.g., CH_3OH) and a decrease in its removal by OH (due to increased [VOC] loading). Additionally, radical concentrations are increased because increasing [VOC] within the smoke plume leads to an increase in the overall rate of the tropospheric photochemical cycle outlined in section 2, and this cycle has the capability to produce more radicals than it consumes [*Crutzen*, 1995; *Holzinger et al.*, 1999; *Field et al.*, 2000].

Table 5. Lifetime of NO_x. Calculated as the Time Required for [NO_x] to Fall to 1/*e* of Its Initial Value

	Simulation	Lifetime (hours)
$\Delta[NO]_0/\Delta[CO]_0 = 1\%$	No Oxy	1.57
	All Oxy	0.57
$\Delta[NO]_0/\Delta[CO]_0 = 2\%$	No Oxy	2.17
	All Oxy	1.16

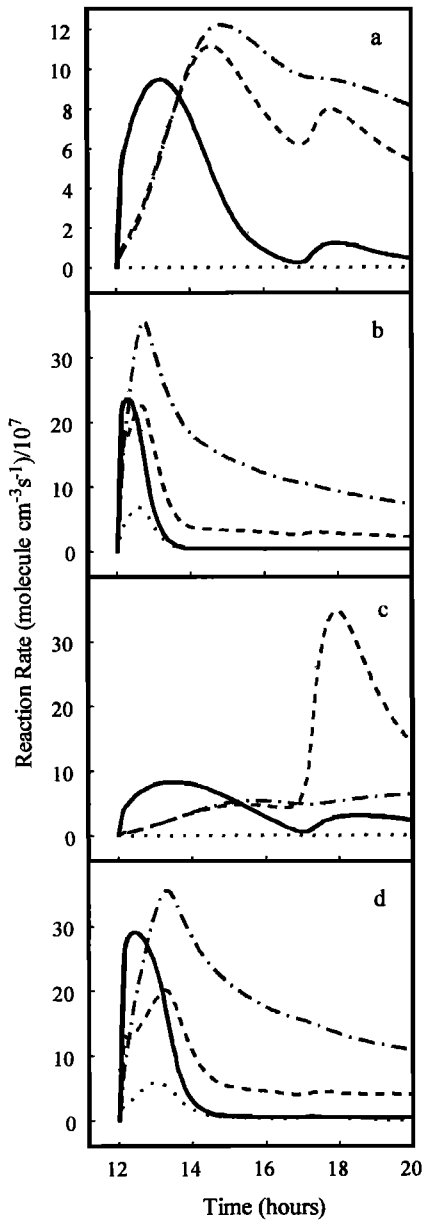

Figure 5. Component reaction rates (molecules/cm^3 s/10^7) of the Rad + NO_x reactions. $RC(O)O_2 + NO_2 \rightarrow$ PANs, dotted-dashed lines; Phenol + $NO_2 \rightarrow$ Nitrophenols, dotted lines; $OH + NO_2 \rightarrow HNO_3$, solid lines; and $RO_2 + NO \rightarrow RONO_2$, dashed lines. (a) No Oxy with $\Delta[NO]_0/\Delta[CO]_0 = 1\%$; (b) All Oxy with $\Delta[NO]_0/\Delta[CO]_0 = 1\%$; (c) No Oxy with $\Delta[NO]_0/\Delta[CO]_0 = 2\%$; (d) All Oxy with $\Delta[NO]_0/\Delta[CO]_0 = 2\%$. All traces show an initial dominance of HNO_3 formation which is eventually surpassed by the formation of PANs and $RONO_2$. There is an additional contribution to NO_x removal in the All Oxy simulations owing to the production of nitrophenols.

4.6. Increase in Hydroperoxides

The increased abundance of radical species due to the addition of oxygenates also increases the Rad + Rad termination reactions (Table 6), leading to an increase in overall and maximum hydroperoxide (H_2O_2 and ROOH) production via reactions (4) and (5) (Table 7). This dramatic increase in hydroperoxides represents another oxygenates-based alteration of the product distribution

Table 6. Average Reaction Rates Over a 30-Hour Simulation and the Percent Change Between No Oxy and All Oxy Cases With $\Delta[NO]_0/\Delta[CO]_0 = 1\%$ and 2%

Reactions	Average Reaction Rates, molecules/cm^3 s				Change, %	
	$\Delta[NO]_0/\Delta[CO]_0 = 1\%$		$\Delta[NO]_0/\Delta[CO]_0 = 2\%$			
	No Oxy	All Oxy	No Oxy	All Oxy	$\Delta[NO]_0/\Delta[CO]_0 = 1\%$	$\Delta[NO]_0/\Delta[CO]_0 = 2\%$
Rad + NO_x (Net)[a]	1.03×10^8	9.84×10^7	1.17×10^8	1.47×10^8	−5	26
$RC(O)O_2 + NO_2 \rightarrow$ PANs	5.47×10^7	6.45×10^7	4.63×10^7	9.19×10^7	18	98
$HO + NO_2 \rightarrow HNO_3$	9.55×10^6	7.29×10^6	1.38×10^7	1.45×10^7	−24	5
$RO_2 + NO \rightarrow RONO_2$	3.85×10^7	2.36×10^7	5.67×10^7	3.72×10^7	−39	−34
$ROH + NO_2 \rightarrow$ Nitrophenols	0.0	3.10×10^6	0.0	3.41×10^6	N/A[b]	N/A[b]
NO-to-NO_2 Conversion	1.12×10^8	1.09×10^8	1.02×10^8	1.52×10^8	−3	50
$CH_2O + h\nu$	1.75×10^7	3.02×10^7	1.66×10^7	3.07×10^7	72	85
Rad + Rad	2.63×10^7	5.51×10^7	2.14×10^7	4.75×10^7	110	122
$HO_2 + O_3 \rightarrow HO + 2O_2$	7.86×10^6	1.26×10^7	4.86×10^6	1.43×10^7	60	195

[a] the $HO_2 + NO_2 \rightleftarrows HNO_4$ reaction has been excluded because it occurs equally in both directions.
[b] N/A, not applicable.

profile and has important implications for regional and global tropospheric chemistry. Hydroperoxides act as a reservoir of HO_x and transport of hydroperoxides from the lower to the upper troposphere has been postulated in order to provide an additional HO_x source required to sustain calculated HO_x levels comparable to those actually measured [*Wennberg et al.*, 1998]. Our results indicate that biomass combustion may represent an important source of hydroperoxides resulting from photochemical processing within smoke plumes. Increased H_2O_2 concentrations may have additional significance for heterogeneous chemistry by increasing sulphate aerosol formation and cloud condensation nuclei concentrations [*von Salzen et al.*, 2000].

Table 7. Average Concentrations over a 30-Hour Simulation Period, Total Number of Molecules Present (Plume Volume × Concentration) at the First Day Maximum and After 30 Hours, and Percent Change Between the No-Oxy and All-Oxy Cases With $\Delta[NO]_0/\Delta[CO]_0 = 1\%$ and 2%

Species	$\Delta[NO]_0/\Delta[CO]_0 = 1\%$		$\Delta[NO]_0/\Delta[CO]_0 = 2\%$		Change, %	
	No Oxy	All Oxy	No Oxy	All Oxy	$\Delta[NO]_0/\Delta[CO]_0 = 1\%$	$\Delta[NO]_0/\Delta[CO]_0 = 2\%$
	Concentration, ppbv					
[Total radical species]	0.079	0.113	0.084	0.105	44	25
[OH]	0.00010	0.00007	0.00009	0.00010	−30	13
$[HO_2]$	0.043	0.067	0.035	0.062	55	75
$[RO_2 + RC(O)O_2]$	0.036	0.047	0.049	0.043	30	−11
$[O_3]$	155	137	105	176	−11	68
[PANs]	6.12	7.04	5.23	10.1	15	93
	Total Production at Day 1 Maximum, molecules					
H_2O_2	2.28×10^{26}	1.41×10^{27}	7.90×10^{25}	1.09×10^{27}	519	1275
ROOH	9.24×10^{26}	2.19×10^{27}	7.42×10^{26}	1.68×10^{27}	137	126
HO_2	4.90×10^{24}	1.04×10^{25}	1.29×10^{24}	1.02×10^{25}	113	690
OH	2.23×10^{22}	1.95×10^{22}	1.08×10^{22}	2.52×10^{22}	−13	135
O_3	1.63×10^{28}	1.17×10^{28}	1.04×10^{28}	1.61×10^{28}	−28	54
PANs	7.96×10^{26}	1.06×10^{27}	7.67×10^{26}	1.44×10^{27}	34	88
	Total Production at End of 30 Hours, molecules					
H_2O_2	4.31×10^{26}	2.50×10^{27}	1.23×10^{26}	1.89×10^{27}	479	1437
ROOH	1.44×10^{27}	4.37×10^{27}	1.16×10^{27}	3.43×10^{27}	203	197
O_3	2.67×10^{28}	2.16×10^{28}	1.50×10^{28}	2.81×10^{28}	−19	88
PANs	1.22×10^{27}	1.02×10^{27}	1.25×10^{27}	1.63×10^{27}	−16	30

4.7. Net O_3 Production

It has previously been reported that net O_3 production is largely independent of [VOC] under NO_x sensitive conditions [*Sillman*, 1999]. However, our simulations show that the net effect of directly emitted oxygenates on overall O_3 production is quite complex owing to the increase in radical species concentrations and subsequent increase in the rate of removal of NO_x from the plume via Rad + NO_x reactions.

Because O_3 production ($O_2 + O^3P \rightarrow O_3$) results from the photolysis of NO_2 (to yield NO + O^3P), the decrease in NO_x lifetime due to the addition of oxygenates is mimicked by O_3 production (Table 8) under both NO emission scenarios. Net O_3 production, however, takes into account changes in O_3 destruction, as well as O_3 production. In the MM there are a total of 20 O_3 destruction reactions. The primary O_3 destruction reaction rates, combined as in Table 8, are shown in Figure 6. Overall O_3 destruction decreases owing to the addition of the oxygenates for both NO emission scenarios (Table 8). This is mainly due to a decrease in the $NO_x + O_3$ reactions (Table 8), an effect that naturally follows from the decrease in NO_x lifetime. The decrease in O_3 destruction due to reaction with NO_x is slightly counteracted by an increase in O_3 destruction due to reaction with HO_2 (Table 8). Both *Field et al.* [2000] and *Crutzen* [1995] have noted the importance of the $HO_2 + O_3$ reaction with respect to O_3 depletion in NO_x-poor environments. Hence both O_3 destruction and O_3 production are reduced owing to the addition of the oxygenated organic species, and net O_3 production results from a balancing of these two effects.

4.8. Complex Effects on O_3 and OH

In the lower initial NO_x simulations ($\Delta[NO]_0/\Delta[CO]_0 = 1\%$), the increased removal of NO_x due to the addition of oxygenates causes a decrease in the average NO-to-NO_2 conversion rates (Table 6) and thus a decrease in the concentrations and production of O_3 and OH (Table 7). However, in the higher initial NO_x models the increased removal of NO_x is balanced by its increased initial concentration, and the average NO-to-NO_2 conversion rates are in fact increased (Table 6), and so are O_3 and OH (Table 7). Therefore unlike previous VOC-NO_x models which found little dependence of O_3 production upon VOC emissions under NO_x sensitive atmospheric processing conditions [*Sillman*, 1999], the smoke plume simulations reported here indicate a very complex relationship between O_3 formation and the initial concentrations of, at least, oxygenated organic compounds. Under certain conditions an increase in [VOC] through the addition of oxygenated organic species leads to an overall decrease in net O_3 production, while under other circumstances an equivalent increase in [VOC] leads to an increase in net O_3 production. The overall relationship between [VOC] and O_3 production is dictated by the available NO_x, as might be expected from the NO_x sensitive conditions which dominate the oxygenated smoke plume photochemical simulations presented here. We believe the complexity which arises in the VOC-O_3 relationship owing to the direct emission of oxygenated organic species occurs not only because of increased VOC loading by highly reactive species to the system, but also because of the ability of oxygenates to photolyze, a pathway which is not available to hydrocarbons, leading to a direct source of radical species.

Table 8. Average O_3 Destruction, O_3 Production, and Net O_3 Production Rates Over 30-Hour Simulation, and the Percent Change between No Oxy and All Oxy Cases with $\Delta[NO]_0/\Delta[CO]_0 = 1\%$ and 2%

	Reaction Rates, molecules/cm^3 s				Change, %	
	$\Delta[NO]_0/\Delta[CO]_0 = 1\%$		$\Delta[NO]_0/\Delta[CO]_0 = 2\%$			
Reaction	No Oxy	All Oxy	No Oxy	All Oxy	$\Delta[NO]_0/\Delta[CO]_0 = 1\%$	$\Delta[NO]_0/\Delta[CO]_0 = 2\%$
O_3-Destruction						
Individual Reactions						
$h\nu + O_3 \rightarrow O(^3P)$	8.48×10^8	8.31×10^8	6.41×10^8	1.04×10^9	−2	62
$h\nu + O_3 \rightarrow O(^1D)$	6.41×10^7	6.63×10^7	5.05×10^7	8.06×10^7	4	60
$NO + O_3 \rightarrow NO_2 + O_2$	9.63×10^8	3.34×10^8	1.92×10^9	8.64×10^8	−65	−55
$NO_2 + O_3 \rightarrow NO_3 + O_2$	1.15×10^7	5.49×10^6	1.90×10^7	1.22×10^7	−52	−36
$NO_2 + O_2 \rightarrow NO + 2O_2$	3.48×10^5	1.66×10^5	5.76×10^5	3.71×10^5	−52	−36
$HO + O_3 \rightarrow HO_2 + O_2$	6.38×10^5	4.46×10^5	4.18×10^5	7.83×10^5	−30	88
$HO_2 + O_3 \rightarrow HO + 2O_2$	7.86×10^6	1.26×10^7	4.86×10^6	1.43×10^7	60	195
$C_2H_4 + O_3 \rightarrow$ [a]	2.89×10^6	3.64×10^6	2.40×10^6	3.49×10^6	26	46
$C_3H_6 + O_3 \rightarrow$ [a]	8.55×10^5	1.20×10^6	7.85×10^5	9.83×10^5	41	25
ud41 + $O_3 \rightarrow$ [a,b]	0.00	8.46×10^2	0.00	6.54×10^2	N/A[c]	N/A[c]
Combined Reactions						
Total Photolysis	9.12×10^8	8.97×10^8	6.92×10^8	1.12×10^9	−2	61
Total NO_x	9.75×10^8	3.39×10^8	1.94×10^9	8.77×10^8	−65	−55
Total HO_x	8.50×10^6	1.31×10^7	5.28×10^6	1.51×10^7	54	187
Total VOC	3.75×10^6	4.84×10^6	3.18×10^6	4.48×10^6	29	41
Total O_3 Destruction	1.90×10^9	1.25×10^9	2.64×10^9	2.01×10^9	−34	−24
Total O_3 Production						
From $O_2 + O(^1P) \rightarrow O_3$	1.98×10^9	1.33×10^9	2.69×10^9	2.11×10^9	−33	−22
Net O_3 Production	7.56×10^7	7.65×10^7	5.22×10^7	1.00×10^8	1	92

[a]First product is an epoxide leading eventually to carbonyl compounds.
[b]Here ud41 ≡ HCOCH = CHCHO.
[c]N/A, not applicable.

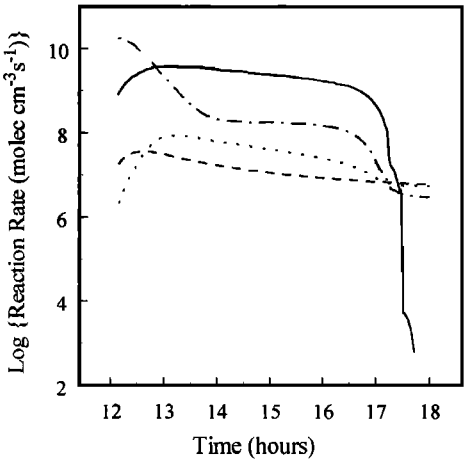

Figure 6. Log of combined O_3 destruction reaction rates (molecules/ cm^3 s) versus time (hours) for the All-Oxy, $\Delta[NO]_0/\Delta[CO]_0$ = 1%, simulation. Total photolysis, solid line; total NO_x, dotted-dashed line; total HO_x, dotted line; total VOC, dashed line.

5. Comparison With Measurements

It is difficult to make valid quantitative comparisons between existing field measurements and our calculated species concentrations. This is because of the simplifications contained within our model and the rarity of appropriate measurements in isolated plumes only hours old. In order to keep the number of reactions manageable, while taking advantage of the detailed chemistry of the MM, we have restricted VOCs to lighter species containing three or less carbon atoms. These lightweight compounds probably represent the majority (by molecule) of HC emissions [*Lobert et al.*, 1991; *Hao et al.*, 1996], but they do not account for the full range of typical emissions. Additionally, our assumed clear-sky conditions could only be strictly representative of the upper levels of a smoke plume. Finally, our model neglects aerosol chemistry, which undoubtedly is a significant perturbation considering the high water solubility of some product species (e.g., hydroperoxides), as well as the high concentrations (up to milligrams per cubic meter) of particulates and water vapor present in a smoke plume.

In light of these and other assumptions, our main purpose then is to compare the results of smoke plume simulations obtained by using a standard initial profile of chemical species with and without added oxygenated organic species. The major result of added oxygenates is found to be increased production of nitrophenols and PANs (Table 7), leading to a decrease in NO_x lifetime within the smoke plume. Validation of these results would require accurate measurements of these organic species in biomass combustion affected air. We are aware of no such data, and our results suggest the need for measurement of these species, as well as investigation of their tropospheric chemistry.

Despite these difficulties, it is possible to make some comparisons. Our calculated values for excess H_2O_2 in Table 3 are reasonably close to the 10 ppbv obtained in limited measurements "near" biomass combustion plumes at altitudes of less than 2 km during Transport and Atmospheric Chemistry Near the Equator-Atlantic (TRACE-A) as reported by *Lee et al.* [1998]. This agreement is obtained without assuming any direct production of H_2O_2 from the fire itself. It also is consistent with TRACE-A analysis by *Mauzerall et al.* [1998], who reported an inability to find evidence of direct emissions of hydroperoxides from biomass combustion but indicated that their net photochemical production within the smoke plume is sufficient to maintain enhancement ratios significantly above ambient, as is also found in our simulations. Furthermore, our calculated values for $\Delta[O_3]/\Delta[CO]$ of ≈8% after 2.5 hours of photochemical processing are consistent with the 7.9 ± 2.4% $\Delta[O_3]/\Delta[CO]$ measured 2.2 ± 1 hours downwind in Alaskan smoke plumes with an average $\Delta[NO]_0/\Delta[CO]_0$ of ≈1.5% [*Goode et al.*, 2000]. Also present in these data is evidence of an initial, very rapid decrease in $\Delta[NH_3]/\Delta[CO]$ with a lifetime of 2.5 hours. While our predicted lifetime for this ratio is somewhat longer than this, the initial rapid decline is clearly present, especially in All-Oxy simulations. Similarly, we find an increase in $\Delta[HCOOH]/\Delta[CO]$ in All-Oxy simulations as the plume evolves, as has been reported [*Goode et al.*, 2000; *Mauzerall et al.*, 1998]. Although our calculated absolute values of this ratio do not agree particularly well with the limited observations, this is not surprising, because our model was not designed to specifically replicate either situation. When a comparison is possible, the addition of oxygenates does seem to improve agreement with measurement; however, there is not yet an experimental data set with sufficient detail to determine if the simulations are truly better with or without oxygenates.

6. Conclusion

Oxygenated organic compounds have been reported to be ubiquitous components of urban atmospheres and the free troposphere [*Lewis et al.*, 2000; *Singh et al.*, 1995; *Tanner et al.*, 1988], as well as the biomass combustion smoke plumes central to the work reported here. We have incorporated six oxygenates (formaldehyde, acetic acid, formic acid, methanol, phenol, and hydroxyacetaldehyde), which have been identified to be present in the largest amounts in biomass combustion emissions [*Griffith et al.*, 1991; *Yokelson et al.*, 1996a, 1996b, 1997, 1999a; *Goode et al.*, 1999; *Goode et al.*, 2000], into photochemical simulations of the evolution of a smoke plume. There remain oxygenated and hydrocarbon-based species, such as terpenes, present in biomass combustion smoke [*Yokelson et al.*, 1996a, 1996b; *Goode et al.*, 1999] which have not been included in the simulations reported here owing mainly to uncertainties in their abundance and photochemistry.

The primary effect of the addition of oxygenated organic species into biomass combustion smoke plumes is to cause a decrease in NO_x lifetime by a factor of ~2 via Rad + NO_x termination reactions. The formation of PANs and nitrophenols represents a significant portion of the increase in Rad + NO_x reactions due to oxygenate addition. Since All-Oxy simulations occur under primarily NO_x sensitive conditions, the increased availability of radicals also leads to an increase in hydroperoxide concentrations via Rad + Rad termination reactions. The increase in hydroperoxides, as well as the preference for PAN formation over HNO_3, are of interest as these species are longer-term pollutant reservoirs of HO_x and NO_x, respectively, released into a regional atmosphere by biomass combustion.

The depletion of NO_x (via the addition of oxygenated organic species) in an environment which is already NO_x sensitive results in complex behavior of [O_3] and [OH], depending upon initial [NO_x]. When the initial [NO_x] is large enough to compensate for the increased removal of NO_x, the addition of oxygenates leads to an overall increase in the NO-to-NO_2 conversion reactions and therefore an increase in O_3 and OH (as shown in the $[NO]_0/[CO]_0$ = 2% simulations reported here). However, lower initial NO_x concentrations may not be able to compensate for the increased removal of NO_x, leading to a decrease in NO-to-NO_2 conversion

and a subsequent decrease in O_3 and OH (as exemplified in the $[NO]_0/[CO]_0$ = 1% simulations reported here). This intriguing result is contrary to previous VOC-NO_x models which show little dependence of O_3 production on [VOC] under NO_x sensitive conditions. This difference is attributed to the ability of the oxygenates to photolyze, resulting in an additional direct source of radical species which may not be compensated for by the $[NO_x]$ emissions.

These results demonstrate that directly emitted oxygenated organic species alter the product distribution profile, including affecting longer-lived species such as O_3, PANs, and hydroperoxides. Hence simulations intending to predict the quantities of various pollutants injected into regional atmospheres by biomass combustion, as well as those looking to understand the effects of biomass combustion on a global scale, need to include both direct emissions of oxygenated organic materials and a good estimate of initial $[NO_x]$.

Acknowledgments. This work was supported by the NASA Earth System Science Fellowship Program (ESS/98-0000-0184) (to S.A.A.) and by the National Science Foundation (ATM-9819295). The authors wish to thank the National Center for Atmospheric Research, Atmospheric Chemistry Division, Boulder, Colorado, especially Sasha Madronich and Peter Hess, for their contributions to this work, including access to the NCAR Master Mechanism, many helpful conversations, and sabbatical support to R.J.F. Changes in numerical detail were made in this manuscript between refereeing and publication owing to a correction of rate constant values that had little effect upon our major conclusions.

References

Babbitt, R. E., D. E. Ward, R. A. Susott, W. M. Hao, and S. P. Baker, Smoke from western wildfires, 1994, in *Fire Management Under Fire (Adapting to Change): Proceedings of the 1994 Interior West Fire Council Meeting and Program*, edited by K. Close and R. A. Bartlette, pp. 51-60, Int. Assoc. of Wildland Fire, Fairfield, Wash., 1998.

Brasseur, G. P., J. J. Orlando, and G. S. Tyndall, *Atmospheric Chemistry and Global Change*, Oxford Univ. Press, New York, 1999.

Chatfield, R. B., and A. C. Delany, Convection links biomass burning to increased tropical ozone: However, models will tend to overpredict O_3, *J. Geophys. Res.*, *95*, 18,473-18,488, 1990.

Chatfield, R. B., J. A. Vastano, H. B. Singh, and G. W. Sachse, A general model of how fire emissions and chemistry produce African/oceanic plumes (O_3, CO, PAN, smoke) in TRACE-A, *J. Geophys. Res.*, *101*, 24,279-24,306, 1996.

Crutzen, P. J., Overview of tropospheric chemistry: Developments during the past quarter century and a look ahead, *Faraday Discuss.Chem. Soc.*, *100*, 1-21, 1995.

Crutzen, P. J., and M. O. Andreae, Biomass burning in the tropics: Impact on atmospheric chemistry and geochemical cycles, *Science*, *250*, 1669-1678, 1990.

Crutzen, P. J., and G. R. Carmichael, Modeling the influence of fire on atmospheric chemistry, in *Fire in the Environment: The Ecological, Atmospheric and Climatic Importance of Vegetative Fires*, edited by P. J. Crutzen and J. G. Goldhammer, pp. 89-105, John Wiley, New York, 1993.

Csanady, G. T., *Turbulent Diffusion in the Environment*, D. Reidel, Norwell, Mass., 1973.

Daum, P. H., Kleinman, L. I., Imre, D., Nunnermacker, L. J., Lee, Y.-N., Springston, S. R., and Newman, L., Analysis of O_3 formation during a stagnation episode in central Tennessee in summer 1995, *J. Geophys. Res.* *105*, 9107-9119, 2000.

Field, R. J., P. G. Hess, L. V. Kalachev, and S. Madronich, Characterization of oscillation and a period-doubling transition to chaos reflecting dynamic instability in a simplified model of tropospheric chemistry, *J. Geophys. Res.*, in press, 2001.

Finlayson-Pitts, B. J., and J. N. Pitts, *Atmospheric Chemistry: Fundamentals and Experimental Techniques*, John Wiley, New York, 1986.

Finlayson-Pitts, B. J., and J. N. Pitts, *Chemistry of the Upper and Lower Atmosphere*, Academic, San Diego, Calif., 2000.

Gifford, F. A., Horizontal diffusion in the atmosphere: A Lagrangian-dynamical theory, *Atmos. Environ.*, *16*, 505-512, 1982.

Goode, J. G., R. J. Yokelson, R. A. Susott, and D. E. Ward, Trace gas emissions from laboratory biomass fires measured by open-path Fourier transform infrared spectroscopy: Fires in grass and surface fuels, *J. Geophys. Res.*, *104*, 21,237-21,245, 1999.

Goode, J. G., R. J. Yokelson, D. E. Ward, R. A. Susott, R. E. Babbitt, M. A. Davies, and W. M. Hao, Measurements of excess O_3, CO_2, CO, CH_4, C_2H_4, C_2H_2, HCN, NO, NH_3, HCOOH, CH_3COOH, HCHO, and CH_3OH in 1997 Alaskan biomass burning plumes by airborne Fourier transform infrared spectroscopy (AFTIR), *J. Geophys. Res.*, *105*, 22,147-22,166, 2000.

Griffith, D. W. T., W. G. Mankin, M. T. Coffey, D. E. Ward, and A. Riebau, FT-IR remote sensing of biomass burning emissions of CO_2, CO, CH_4, CH_2O, NO, NO_2, NH_3, and N_2O, in *Global Biomass Burning: Atmospheric, Climatic and Biospheric Implications*, edited by J. S. Levine, pp. 230-239, MIT Press, Cambridge, Mass., 1991.

Hao, W. M., and M.-H. Liu, Spatial and temporal distribution of tropical biomass burning, *Global Biogeochem. Cycles*, *8*, 495-503, 1994.

Hao, W. M., D. E. Ward, G. Olbu, and S. P. Baker, Emissions of CO_2, CO, and hydrocarbons from fires in diverse African savanna ecosystems, *J. Geophys. Res.*, *101*, 23,577-23,584, 1996.

Hindmarsh, A. C., ODEPACK: A systematized collection of ODE solvers, in *Scientific Computing*, edited by R. S. Stepleman, pp. 55-64, North-Holland, New York, 1983.

Holzinger, R., C. Warneke, A. Hansel, A. Jordan, W. Lindinger, D. H. Scharffe, G. Schade, and P. J. Crutzen, Biomass burning as a source of formaldehyde, acetaldehyde, methanol, acetone, acetonitrile, and hydrogen cyanide, *Geophys. Res. Lett.*, *26*, 1161-1164, 1999.

Jacob, D. J., et al., Summertime photochemistry of the troposphere at high northern latitudes, *J. Geophys. Res.*, *97*, 16,421-16,431, 1992.

Jacob, D. J., et al., Origin of ozone and NO_x in the tropical troposphere: A photochemical analysis of aircraft observations over the south Atlantic basin, *J. Geophys. Res.*, *101*, 24,235-24,250, 1996.

Keller, M., D. J. Jacob, S. C. Wofsy, and R. C. Harriss, Effects of tropical deforestation on global and regional atmospheric chemistry, *Clim. Change*, *19*, 139-158, 1991.

Kleinman, L. I., Low and high NO_x tropospheric photochemistry, *J. Geophys. Res.*, *99*, 16,831-16,838, 1994.

Kleinman, L. I., Daum, P. H., Lee, J. H., Lee, Y.-N., Nunnermacker, L. J., Springston, S. R., and Newman, L., Dependence of ozone production on NO and hydrocarbons in the troposphere, *Geophys. Res. Lett.*, *24*, 2299-2302, 1997.

Kley, D., Tropospheric chemistry and transport, *Science*, *276*, 1043-1045, 1997.

Koppmann, R., A. Khedim, J. Rudolph, D. Poppe, M. O. Andreae, G. Helas, M. Welling, and T. Zenker, Emissions of organic trace gases from savanna fires in southern Africa during the 1992 Southern Africa Fire Atmosphere Research Initiative and their impact on the formation of tropospheric ozone, *J. Geophys. Res.*, *102*, 18,879-18,888, 1997.

Lee, M., B. G. Heikes, and D. J. Jacob, Enhancements of hydroperoxides and formaldehyde in biomass burning impacted air and their effect on atmospheric oxidant cycles, *J. Geophys. Res.*, *103*, 13,201-13,212, 1998.

Lewis., A. C., N. Carslaw, P. J. Marriott, R. M. Kinghorn, P. Morrison, A. L. Lee, K. D. Bartle, and M. J. Pilling, A larger pool of ozone-forming carbon compounds in urban atmospheres, *Nature*, *405*, 778-781, 2000.

Lobert, J. M., D. H. Scarffe, W. M. Hao, T. A. Kuhlbusch, R. Seuwen, P. Warneck, and P. J. Crutzen, Experimental evaluation of biomass burning emissions: Nitrogen and carbon containing compounds, in *Global Biomass Burning: Atmospheric, Climatic, and Biospheric Implications*, edited by J. S. Levine, pp. 289-304, MIT Press, Cambridge, Mass., 1991.

Madronich, S., Photodissociation in the atmosphere, 1, Actinic flux and the effects of ground reflection and clouds, *J. Geophys. Res.*, *92*, 9740-9752, 1987.

Madronich, S., and J. G. Calvert, The NCAR master mechanism of gas phase chemistry-version 2.0, *NCAR Tech. Note*-333+STR, Natl. Cent. for Atmos. Res., Boulder, Colo., 1989.

Mauzerall, D. L., J. A. Logan, D. J. Jacob, B. E. Anderson, D. R. Blake, J. D. Bradshaw, B. Heikes, G. W. Sachse, H. Singh, and B. Talbot, Photochemistry in biomass burning plumes and implications for tropospheric ozone over the tropical south Atlantic, *J. Geophys. Res.*, *103*, 8401-8423, 1998.

McKenzie, L., W. M. Hao, G. N. Richards, and D. E. Ward, Measurement and modeling of air toxins from smoldering combustion of biomass, *Environ. Sci. Technol.*, *29*, 2047-2054, 1995.

Olcese, L. E., and B. M. Toselli, Fast and reliable numerical methods to simulate complex chemical kinetic mechanisms, *Int. J. Chem. Kinet.*, *30*, 349-358, 1998.

Olson, J., et al., Results from the intergovernmental panel on climatic change photochemical model intercomparsion (PhotoComp), *J. Geophys. Res.*, *102*, 5979-5991, 1997.

Poppe, D., R. Koppmann, and J. Rudolph, Ozone formation in biomass burning plumes: Influence of atmospheric dilution, *Geophys. Res. Lett.*, *25*, 3823-3826, 1998.

Richardson, J. L., J. Fishman, and G. L. Gregory, Ozone budget over the Amazon: Regional effects from biomass burning emissions, *J. Geophys. Res.*, *96*, 13,073-13,087, 1991.

Seinfeld, J. H., and S. N. Pandis, *Atmospheric Chemistry and Physics: From Air Pollution to Climate Change*, John Wiley, New York, 1998.

Sillman, S., The use of NO_y, H_2O_2, and HNO_3 as indicators for ozone-NO_x-hydrocarbon sensitivity in urban locations, *J. Geophys. Res.*, *100*, 14,175-14,188, 1995.

Sillman, S., The relation between ozone, NO_x and hydrocarbons in urban and polluted rural environments, *Atmos. Environ.*, *33*, 1821-1845, 1999.

Sillman, S., J. A. Logan, and S. C. Wofsy, A regional scale model for ozone in the United States with subgrid representation of urban and power plant plumes, *J. Geophys. Res.*, *95*, 5731-5748, 1990.

Singh, H. B., M. Kanakidou, P. J. Crutzen, and D. J. Jacob, High concentrations and photochemical fate of oxygenated hydrocarbons in the global troposphere, *Nature*, *378*, 50-54, 1995.

Tanner, R. L., A. H. Miguel, J. B. de Andrade, J. S. Gaffney, and G. E. Streit, Atmospheric chemistry of aldehydes: Enhanced peroxyacetyl nitrate formation from ethanol-fueled vehicular emissions, *Environ. Sci. Technol.*, *22*, 1026-1034, 1988.

Thompson, A. M., K. E. Pickering, D. P. McNamara, M. R. Schoeberl, R. D. Hudson, J. H. Kim, E. V. Browel, V. W. J. H. Kirchoff, and D. Nanga, Where did tropospheric ozone over southern Africa and the tropical Atlantic come from in October 1992? Insight from TOMS, GTE TRACE-A, and SAFARI 1992, *J. Geophys. Res.*, *101*, 24,251-24,278, 1996.

von Salzen, K., H. G. Leighton, P. A. Ariya, L. A. Barrie, S. L. Gong, J.-P. Blanchet, L. Spacek, U Lohmann, and L. I. Kleinman, Sensitivity of sulphate aerosol size distributions and CCN concentrations over North America to SO_x emissions and H_2O_2 concentrations, *J. Geophys. Res.*, *105*, 9741-9765, 2000.

Wennberg. P. O., et al., Hydrogen radicals, nitrogen radicals, and the production of O_3 in the upper troposphere, *Science*, *279*, 49-53, 1998.

Worden, H., R. Beer, and C. P. Rinsland, Airborne infrared spectroscopy of 1994 western wildfires, *J. Geophys. Res.*, *102*, 1287-1299, 1997.

Yokelson, R. J., D. W. T. Griffith, and D. E. Ward, Open-path FT-IR studies of large-scale laboratory biomass fires, *J. Geophys. Res.*, *101*, 21,067-21,080, 1996a.

Yokelson, R. J., D. W. T. Griffith, J. B. Burkholder, and D. E. Ward, Accuracy and advantages of synthetic calibration of smoke spectra, in *Optical Remote Sensing for Environmental and Process Monitoring*, pp. 365-376, Air and Waste Manage. Assoc., Pittsburgh, Pa.,1996b.

Yokelson, R. J., D. E. Ward, R. A. Susott, J. Reardon, and D. W. T. Griffith, Emissions from smoldering combustion of biomass measured by open-path Fourier transform infrared spectroscopy, *J. Geophys. Res.*, *102*, 18,865-18,877, 1997.

Yokelson, R. J., J. G. Goode, D. E. Ward, R. A. Susott, R. E. Babbitt, D. D. Wade, I. Bertschi, D. W. T. Griffith, and W. M. Hao, Emissions of formaldehyde, acetic acid, methanol, and other trace gases from biomass fires in North Carolina measured by airborne Fourier transform infrared spectroscopy, *J. Geophys. Res.*, *104*, 30,109-30,125, 1999a.

Yokelson, R. J., R. A. Susott, R. E. Babbitt, D. E. Ward, and W. M. Hao, Trace gas emissions from specific biomass fire-types, in *START Synthesis Workshop on Greenhouse Gas Emission, Aerosols and Land Use and Cover Change in Southeast Asia*, edited by T. Moya, pp. 60-68, SARCS, IGAC, LUCC, IGBP China-Taipei, Taipei, Taiwan, 1999b.

S. A. Mason, R. J. Field, M. A. Kochivar, M. R. Tinsley, and R. J. Yokelson, Department of Chemistry, The University of Montana, Missoula, MT 59812. (arrieta@selway.umt.edu; ch_rjf@selway.umt.edu; taslhoff@selway.umt.edu; markt@selway.umt.edu;byok@selway.umt.edu)

W. M. Hao and D. E. Ward, USDA Forest Service, Rocky Mountain Research Station Fire Sciences Laboratory, Missoula, MT 59807. (whao@fs.fed.us; dward@fs.fed.us)

(Received August 4, 2000; revised November 27, 2000; accepted January 3, 2001.)